International Journal of Heat and Mass Transfer 121 (2018) 1–9

Contents lists available at ScienceDirect

International Journal of Heat and Mass Transfer

journal homepage: www.elsevier.com/locate/ijhmt

Analytical modeling of oscillatory heat transfer in coated sorption beds

Hesam Bahrehmand, Mehran Ahmadi, Majid Bahrami *

Laboratory for Alternative Energy Conversion (LAEC), School of Mechatronic Systems Engineering, Simon Fraser University, Surrey, BC V3T 0A3, Canada

ARTICLE INFO

Article history:
Received 7 July 2017
Accepted 28 December 2017

Keywords:
Oscillatory heat transfer
Sorption cooling system
Analytical modeling
Thermal contact resistance
Thermal diffusivity

ABSTRACT

A novel analytical model that considers the thermal contact resistance (TCR) at the interface between the sorbent layer and heat exchanger (HEX) is developed to investigate the oscillatory heat transfer and performance of coated sorption beds. The governing energy equation is solved using an orthogonal expansion technique and closed-form relationships are obtained to calculate the temperature distribution inside the sorbent coating and HEX. In addition, a new gravimetric large pressure jump (GLAP) test bed is designed to measure the uptake of sorption material. Novel graphite coated sorption beds were prepared and tested in the GLAP test bed. The model was successfully validated with the measurements performed in the GLAP test bed. It is found that specific cooling power (SCP) of a sorption cooling system (SCS) enhances by increasing the sorbent thermal diffusivity and decreasing the TCR. For example, SCP of the sorption cooling system (SCS) can be enhanced from 90 to 900 (W/kg) by increasing the sorbent thermal diffusivity from 2.5e−7 to 5.25e−6 (m^2/s) and decreasing the TCR from 4 to 0.3 (K/W). Moreover, the results show that SCP increases by reducing the HEX to sorbent thickness ratio (HSTR). Therefore, the proposed graphite coated sorption beds with high thermal diffusivity and low thickness are suitable for sorption cooling applications.

1. Introduction

Conventional vapor compression refrigeration systems consume approximately 15% of global electrical energy and have a significant carbon footprint [1]. Sorption cooling systems (SCS), with working pairs such as water and silica gel or $CaCl_2$-silica gel, can be driven with low-grade heat, i.e. temperature sources below 100 °C, which is used to regenerate the sorbent material. However, commercialization of SCS faces fundamental challenges, including: (i) low specific cooling power (SCP), due to poor heat transfer between sorber bed heat exchanger (HEX) [2–4] and the loose grain or coated sorbent, which ultimately leads to large sizes for SCS; and (ii) low coefficient of performance (COP). Granular packed sorbent bed design offers the advantage of higher mass transfer rates and lower cost of manufacturing; nonetheless, heat transfer rate in packed beds are inherently poor due to the point contacts between HEX and grains as well as to the low thermal diffusivity of the sorbent material [5]. Coated sorbent beds can improve heat transfer rate, as there is a higher conductance between the heat exchanger surface and the sorbent material. However, for thin coatings (0.1–5 mm), the relative thermal inertia of the HEX metal mass is considerable, which deteriorates the sorption efficiency and SCP. The importance of HEX thermal inertia results from the oscillatory heat transfer inside the sorber beds. Sorber beds need to be cooled down/heated up during sorption/desorption phases because of their exothermic/endothermic nature, and these oscillatory cool down/heat up processes are performed with the heat transfer fluid flowing through the sorber bed HEX. The oscillatory thermal behavior of SCS makes the thermal diffusivity of the sorbent coating and HEX crucially important in determining its performance. Moreover, the thermal contact resistance between the sorbent (for both coated layer and particles) and the HEX surface is key and can be up to 26% of the bulk thermal resistance inside a sorber bed [6,7]. Thus, the heat transfer characteristics of sorber beds have a tremendous impact on the overall performance, SCP and COP of SCS and should be thoroughly investigated.

Mathematical modeling is a primary tool for design and optimization of sorption cooling systems that if used properly in conjunction with experimental studies, can reduce the cost and save time. The simplest approach to study the sorber beds is thermodynamic modeling. These models are fairly simple and cost-effective; however, they can only predict the upper performance limits of a SCS [8–12].

Another method to investigate the sorption beds is to adopt a lumped model, which is based on the assumptions of a uniform

* Corresponding author at: School of Mechatronic Systems Engineering, Simon Fraser University, 250-13450 102 Avenue, Surrey, BC V3T 0A3, Canada.
E-mail addresses: sbahrehm@sfu.ca (H. Bahrehmand), mahmadi@sfu.ca (M. Ahmadi), mbahrami@sfu.ca (M. Bahrami).

https://doi.org/10.1016/j.ijheatmasstransfer.2017.12.147
0017-9310/

Nomenclature

A	heat transfer area, m^2
c	specific heat capacity, J/kg K
Fo	Fourier number
g_i	dimensionless heat generation
H	enthalpy, J/kg
Ja	Jacob number
k	thermal conductivity, W/m K
p	pressure, Pa
p_0	saturation pressure, Pa
Q	cooling energy, J
R_c	dimensionless thermal contact resistance
T	temperature, K
t	time, s
X	eigenfunction
x	coordinate

Greek symbols

α	thermal diffusivity, m^2/s
β	eigenvalue
Γ	gamma function
η	dimensionless coordinate
κ	dimensionless thermal conductivity ratio
μ	dimensionless thermal diffusivity ratio
θ	dimensionless temperature
ρ	density, kg/m^3
τ	cycle time, s
Ω	dimensionless angular frequency of the sorption cycles
ω	sorbate uptake, g/g dry sorbent

Subscripts

0	initial condition
evap	evaporator/evaporative
sorb	sorbent
sorp	sorption

Abbreviations

COP	coefficient of performance
HEX	heat exchanger
HSTR	HEX to sorbent thickness ratio
GLAP	gravimetric large pressure jump
PVP	polyvinylpyrrolidone
SCP	specific cooling power
SCS	sorption cooling system
TCR	thermal contact resistance
TGA	thermogravimetric Analysis

sorbent temperature, uniform sorption of the refrigerant and thermodynamic equilibrium between the solid and gaseous phases. In such models, inter-particle mass transfer and heat transfer resistances are neglected, while the time derivative terms of temperature and sorbate uptake are considered. Energy balance, mass balance and sorption equilibrium equations are solved to acquire the temperature, pressure and sorbate uptake [13–18].

Finally, heat and mass transfer models take into account the variation of sorbent temperature and sorbate uptake with time and space by including convection and diffusion terms in the governing equations. These models solve four governing equations simultaneously: mass conservation, energy balance, momentum equation, and sorption equilibrium. The complexity and nonlinearity of such coupled partial differential equations exclude the possibility of having an analytical solution. Consequently, numerical methods such as finite difference [19–24], finite volume [25–30] and finite element methods [31] are the only feasible approach, but they require high computational time.

In the present model, the temperature and uptake in sorption bed vary with time and space. The governing equations are solved using an orthogonal expansion technique, which is an analytical approach and can generate closed-form relationships [32]. In addition, this model takes into consideration the TCR between sorbent and HEX while the majority of available studies have neglected it. The present analytical model can accurately predict the oscillatory temperature distribution, heat transfer rate and the performance of coated sorption beds considering the TCR at the sorbent-HEX interface.

2. Governing equations

The solution domain consisting of sorbent coating and HEX is shown schematically in Fig. 1. Initially, the sorbent domain is at temperature $T_{1,0}$ and the HEX is at $T_{2,0}$. Continuity of heat flux as well as temperature jump/drop induced by TCR are considered at the interface between the sorbent coating and HEX. The following is the list of assumptions used in the development of the present model:

- The thickness of sorbent and HEX is uniform and sufficiently small compared to the other dimensions; thus, the energy equation can be assumed one-dimensional;
- The outer surface of the sorbent is assumed adiabatic. The convective heat transfer is negligible due to very low operating pressure (1–5 kPa) and the radiative heat transfer is negligible due to low temperature difference between the sorbent and its surrounding (10–20 K);
- Thermophysical properties of the sorbent and HEX are assumed constant;
- Convective effects of the sorbate inside the sorbent coating are negligible.

As such, the energy equation for the sorption layer and HEX can be written as follows.

$$\alpha_i \frac{\partial^2 T_i(x,t)}{\partial x^2} + \frac{\alpha_i}{k_i} G_i(t) = \frac{\partial T_i(x,t)}{\partial t}, \quad x_{i-1} \leqslant x \leqslant x_i, t > 0 \quad i = 1,2 \tag{1}$$

$$G_i(t) = \begin{cases} \rho_{sorb} H_{sorp} \frac{dw}{dt}, & i = 1 \\ 0, & i = 2 \end{cases} \tag{2}$$

where i = 1 and i = 2 represent the sorbent and HEX domains, respectively. The boundary conditions are

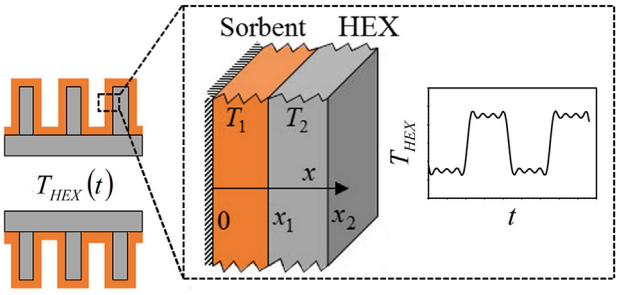

Fig. 1. Schematic diagram of the solution domain consisting of sorbent coating and HEX.

$$\frac{\partial T_1(0,t)}{\partial x} = 0 \tag{3}$$

$$k_1 \frac{\partial T_1(x_1,t)}{\partial x} = k_2 \frac{\partial T_2(x_1,t)}{\partial x} \tag{4}$$

$$-k_1 \frac{\partial T_1(x_1,t)}{\partial x} = \frac{1}{A \cdot TCR}(T_1(x_1,t) - T_2(x_1,t)) \tag{5}$$

$$T_2(x_2,t) = T_{HEX}(t) \tag{6}$$

Furthermore, the initial condition is

$$T_1(x,0) = T_{1,0},\ T_2(x,0) = T_{2,0} \tag{7}$$

The following non-dimensional variables are defined as follows.

$\eta = \frac{x}{x_1}$	$Fo = \frac{\alpha_2 t}{x_1^2}$	$\theta = \frac{T_i(\eta,Fo) - T_{HEX}(Fo)}{T_{2,0}}$
$g_i = \frac{\rho H_{sorp} \alpha_i}{k_i T_0} \frac{dw}{dFo}$	$\kappa_{i+1} = \frac{k_{i+1}}{k_i}$	$R_c = \frac{k_i A \cdot TCR}{x_1}$
$\mu_i = \frac{\alpha_i}{\alpha_2}$		

where θ_i is the dimensionless temperature of the ith layer, the Fourier number, Fo, is the dimensionless time, η is the dimensionless coordinate, g_i is the dimensionless heat generation inside the ith layer and R_c is the dimensionless thermal contact resistance. Using the aforementioned dimensionless variables, the dimensionless energy equation as well as boundary and initial conditions can be obtained as follows.

$$\mu_i \frac{\partial^2 \theta_i(\eta,Fo)}{\partial \eta^2} + g_i(Fo) = \frac{\partial \theta_i(\eta,Fo)}{\partial Fo} + \frac{1}{T_0}\frac{dT_{HEX}(Fo)}{dFo} \tag{8}$$

$$\frac{\partial \theta_1(0,Fo)}{\partial \eta} = 0 \tag{9}$$

$$\frac{\partial \theta_1(1,Fo)}{\partial \eta} = \kappa_2 \frac{\partial \theta_2(1,Fo)}{\partial \eta} \tag{10}$$

$$-\frac{\partial \theta_1(1,Fo)}{\partial \eta} = \frac{1}{R_c}(\theta_1(1,Fo) - \theta_2(1,Fo)) \tag{11}$$

$$\theta_2(x_2/x_1,Fo) = 0 \tag{12}$$

$$\theta_1(\eta,0) = \frac{T_{1,0} - T_{HEX}(0)}{T_{2,0}}, \quad \theta_2(\eta,0) = \frac{T_{2,0} - T_{HEX}(0)}{T_{2,0}} \tag{13}$$

where $T_{HEX}(Fo)$ is the temperature at the outer surface of HEX, which can have any oscillatory profile. Fourier series in the form of Eq. (14) are used to represent this oscillatory variation of HEX temperature.

$$T_{HEX}(Fo) = a_0' + \sum_{j=1}^{4}(a_j' \cos(j\Omega Fo) + b_j' \sin(j\Omega Fo)) \tag{14}$$

$$\Omega = \frac{2\pi}{Fo_{cycle}}$$

where Ω is the dimensionless angular frequency of the sorption cycles.

3. Modeling of sorbate uptake

The present model solves the energy equation in sorber beds; thus, the water uptake (source term in the energy equation) should be modelled in terms of operating conditions of the sorption cycles, to be specific, temperature and pressure. The isotherm plot of the sorbent material, obtained using an IGA-002 thermogravimetric sorption analyzer (TGA) (Hiden Isochema), is indicated in Fig. 2. Sorbent material, consisting of 35 wt% $CaCl_2$, 35 wt% silica gel B150, 10 wt% PVP-40, and 20 wt% graphite flakes, is placed on the sample cell, which is held by a microbalance to measure the mass changes of the sorbent, while the temperature and pressure are controlled. Using curve fitting, a compact relationship is acquired to calculate the uptake as a function of pressure and temperature. Interestingly enough, the relationship between the uptake and temperature can be approximated with a linear function for small temperature jump (<15 °C) as shown by Eq. (15).

$$\omega = m\frac{p}{p_0} + b = m\frac{p}{0.1\exp(20 - 5098/T)} + b \approx m'(p)T + b'(p) \tag{15}$$

where m and b are obtained by fitting a line to the TGA data. Also, m′ and b′ are functions of the operating pressure at sorber bed.

A new gravimetric large pressure jump (GLAP) test bed was custom-built in our lab to verify that the linear relationship between uptake and sorbent temperature obtained from TGA occurs in a real SCS. A schematic diagram of the GLAP test bed is shown in Fig. 3(a). Sorbent material was coated on 0.9 mm thick graphite sheets and installed in the GLAP test bed (Fig. 3(b)). To simulate the operation of a sorption chiller the pressure was stepped from 0.65 kPa to 2.33 kPa while the sample temperature was maintained at 40 °C. The sorber bed was placed on an ML4002E Precision Balance with an accuracy of 0.01 g to measure the mass of the sorbate uptake. K-type thermocouples with an accuracy of 1.1 °C were passed via a feed-through in the vacuum chamber to measure the sorbent temperature. The pressure of the sorber bed and the evaporator/condenser is measured using 722B Baratron pressure transducer with the accuracy of 0.5%. The instruments were interfaced with a PC through a data acquisition system and software built in the LabVIEW environment.

The variation of water uptake versus sorbent temperature measured by GLAP test bed and TGA is shown in Fig. 4. It can be seen that the results are in a good agreement; hence, Eq. (15) can be used to model the sorbate uptake in terms of sorbent temperature and sorber bed pressure.

It was demonstrated that variation of sorbate uptake with sorbent temperature can be approximated with a line for any given pressure of sorber bed. Since sorption cycles operate between two pressures (sorption/desorption), two constant-pressure lines can represent the sorption phases (Fig. 4). At the beginning of sorption/desorption phases, sorbent temperature increases/decreases rapidly at almost constant sorbate uptake until the bed pressure reaches the evaporator/condenser pressure (considering the pressure drop between the evaporator/condenser and the bed); subse-

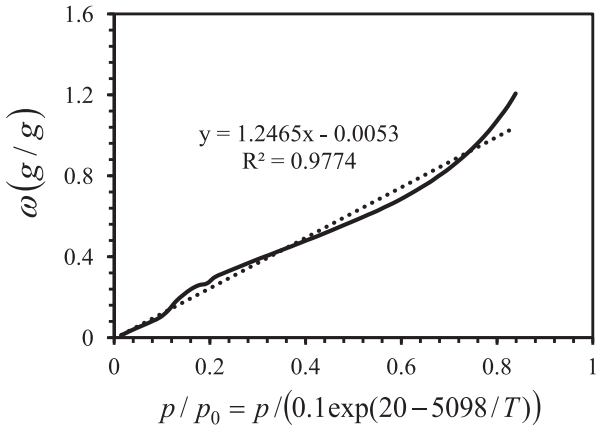

Fig. 2. TGA isotherm data for the sorbent material used.

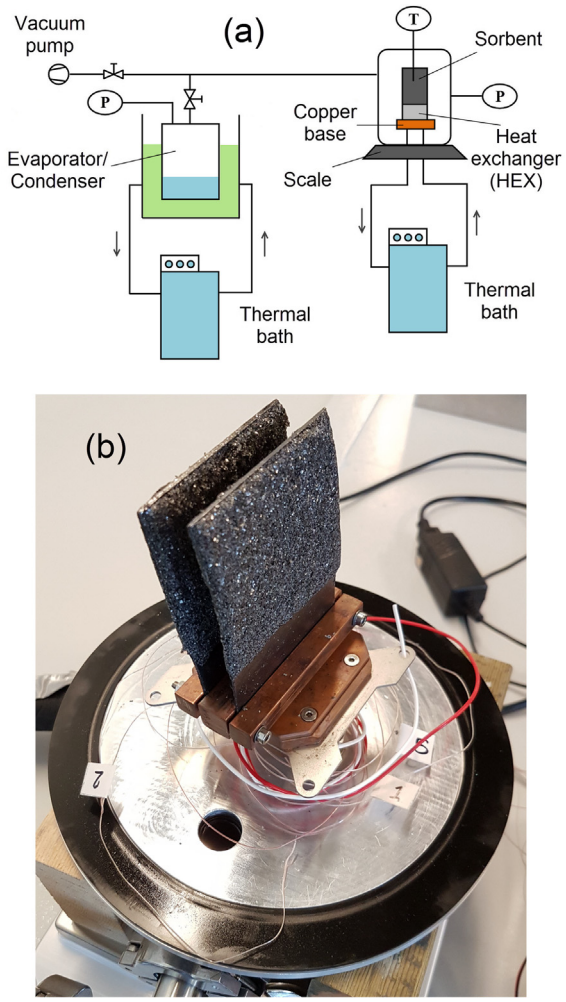

Fig. 3. (a) Schematic diagram of the GLAP test bed, (b) custom-built gravimetric large pressure jump (GLAP) test bed.

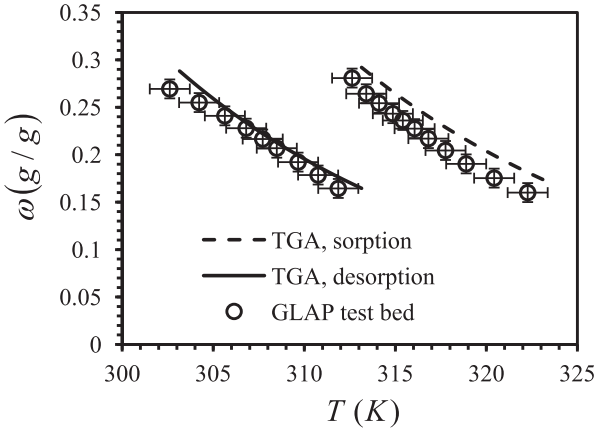

Fig. 4. Water uptake versus sorbent temperature (comparison between the results acquired from GLAP test bed and TGA).

quently, the sorber bed is gradually cooled down/heated up to perform the sorption/desorption phases. The reason why the uptake remains almost constant during this temperature jump/drop process, is shown through a scale analysis on the energy equation in Eq. (16). Therefore, the uptake is assumed constant during this rapid process and the temperature jump/drop is taken into account as initial condition in the energy equation ($T_{1,0}$).

$$\rho c\frac{\partial T}{\partial t}=k\frac{\partial^2 T}{\partial x^2}+\rho H_{sorp}\frac{d\omega}{dt}\overset{Verysmall\ \Delta t}{\Rightarrow}\rho c\frac{\Delta T}{\Delta t}\sim\rho H_{sorp}\frac{\Delta\omega}{\Delta t}$$
$$\Rightarrow\Delta\omega\sim\frac{c\Delta T}{H_{sorp}}=\mathrm{Ja}_{sorp}<0.005 \tag{16}$$

4. Model development

An analytical model was developed to predict the temperature distribution and heat transfer rate inside the sorbent coating and HEX. The methodology of the solution is presented in Appendix A. Performing an integration in Eq. (A20) as well as some algebraic manipulation, the dimensionless temperature of sorbent and HEX can be obtained as follows.

$$\theta_1(\eta,Fo)=\sum_{n=1}^{\infty}\cos\left(\frac{\beta_n}{\sqrt{\mu_1}}\eta\right)\left[f_n^* e^{-\beta_n^2 Fo}+\sum_{j=1}^{4}\left\{r_{j,n}\left(\cos(j\omega Fo)-e^{-\beta_n^2 Fo}\right)+s_{j,n}\sin(j\omega Fo)\right\}\right] \tag{17}$$

$$\theta_2(\eta,Fo)=\sum_{n=1}^{\infty}\left(C_{2n}\cos\left(\frac{\beta_n}{\sqrt{\mu_2}}\eta\right)+D_{2n}\sin\left(\frac{\beta_n}{\sqrt{\mu_2}}\eta\right)\right)\times\left[f_n^* e^{-\beta_n^2 Fo}+\sum_{j=1}^{4}\left\{r_{j,n}\left(\cos(j\omega Fo)-e^{-\beta_n^2 Fo}\right)+s_{j,n}\sin(j\omega Fo)\right\}\right] \tag{18}$$

$$r_{j,n}=\frac{-j\omega I_n^* \beta_n^2}{T_0((j\omega)^2+\beta_n^4)}\left(b_j'+\frac{j\omega a_j'}{\beta_n^2}\right)$$
$$s_{j,n}=\frac{j\omega I_n^* \beta_n^2}{T_0((j\omega)^2+\beta_n^4)}\left(a_j'-\frac{j\omega b_j'}{\beta_n^2}\right)$$

where a'_j and b'_j are the coefficients of the Fourier series fitted to the HEX temperature profile (Eq. (14)).

5. Results and discussion

A code is developed in MATLAB to solve the transcendental equation, Eq. (A5), as well as to calculate the dimensionless temperatures of sorbent and HEX, Eqs. (17) and (18). Our study indicates that the first 3 terms in the series solution (n = 1–3) is accurate enough to yield the temperature distributions up to seven decimal digits.

5.1. Model validation

The thermo-physical properties of sorbent and HEX are presented in Table 1. Moreover, TCR at the silica gel/copper interface was measured by Sharafian et al. [6] using a guarded-hot plate apparatus under vacuum pressure, and the range of 1.3–3.8 K/W was reported. As can be seen in Fig. 5, the SCP values predicted by the present model are in good agreement with those measured with GLAP test bed. It is noted that the main uncertainty in SCP calculation is due to the mass measurement of the sorbate uptake and can result in the uncertainty of 0.5–3.5 W/kg.

5.2. Model discussion

The dimensionless temperature profile inside the sorbent coating and HEX for sorption and desorption phases is depicted on Fig. 6. It is shown that the dimensionless temperature is positive/negative during sorption/desorption phases due to heat generation/removal. In addition, it was found that for thin HEX (see

Table 1
Thermo-physical properties and geometrical characteristics of sorbent and HEX.

	k (W/mK)	ρ (kg/m^3)	c (J/kg K)	H_{sorp} (J/kg)	α (m^2/s)	Thickness (mm)
Sorbent	0.45	1213	1319	2.77e6	2.8e−7	3.4
HEX	5	1550	748	–	4.3e−6	0.9

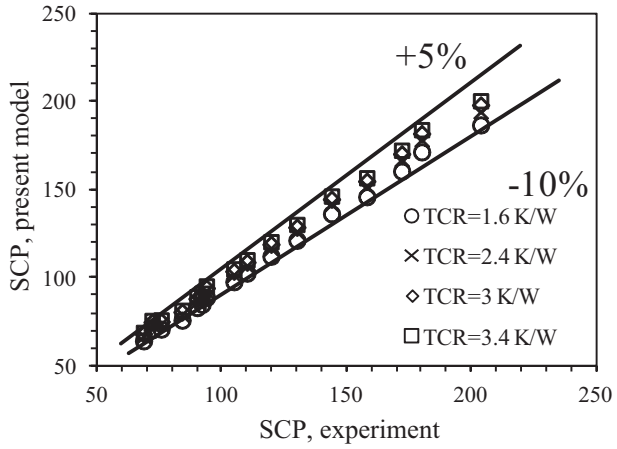

Fig. 5. Validation of the present model with the experimental data.

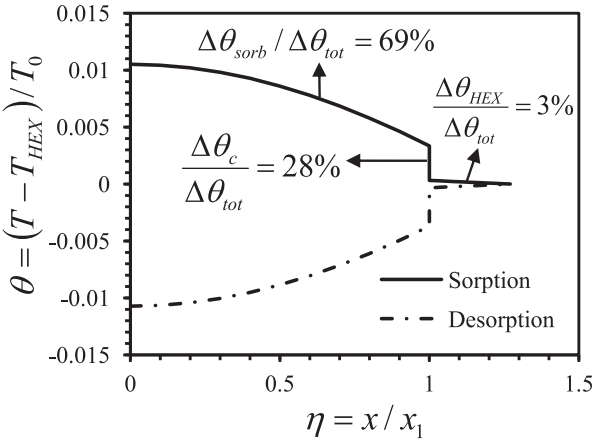

Fig. 6. Dimensionless temperature profile inside the sorbent coating and HEX during sorption and desorption phases.

Table 1) the temperature drop values of sorbent, sorbent/HEX TCR, and the HEX make up 69%, 28% and 3%, respectively, of the total temperature drop inside a sorber bed. The reason behind this is the relatively low sorbent thermal diffusivity, high TCR at the sorbent/HEX interface and high HEX thermal diffusivity (Table 1). The temperature distributions clearly show that sorbent and sorbent–HEX TCR are the main bottlenecks reducing the thermal performance of SCS.

The oscillatory variation of dimensionless temperature at different locations of sorber bed is shown in Fig. 7. It is seen that a sudden temperature jump/drop occurs at the beginning of sorption/desorption phases; afterwards, the sorber bed is gradually cooled down or heated up to perform the sorption/desorption phases. Hence, what determines the SCS performance is how fast the sorber bed can be cooled down/heated up after the temperature jump/drop takes place. That clearly shows the importance of sorbent thermal diffusivity and the impact of TCR at the HEX–sorbent interface.

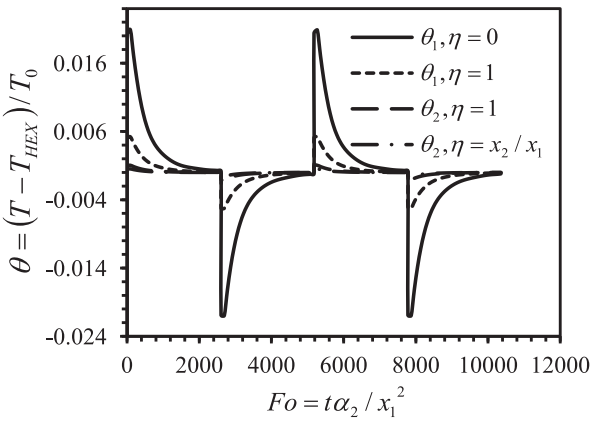

Fig. 7. Oscillatory variation of dimensionless temperature of the sorbent and HEX versus Fo number at different locations of sorber bed.

Table 2
Various oscillatory heat transfer characteristics and geometrical specifications used for parametric study.

Section	α_{sorb} (m^2/s)	TCR (K/W)	α_{HEX} (m^2/s)	HSTR
5.3.1	2.5e−7	1	4e−6	0.25
	2.5e−7	3	4e−6	0.25
	2.5e−7	5	4e−6	0.25
	2.5e−7	7	4e−6	0.25
	2.5e−7	9	4e−6	0.25
5.3.2	1.25e−7	3	4e−6	0.25
	1.875e−7	3	4e−6	0.25
	2.5e−7	3	4e−6	0.25
	3.125e−7	3	4e−6	0.25
	3.75e−7	3	4e−6	0.25
5.3.3	2.5e−7	3	2e−6	0.25
	2.5e−7	3	3e−6	0.25
	2.5e−7	3	4e−6	0.25
	2.5e−7	3	5e−6	0.25
	2.5e−7	3	6e−6	0.25
5.3.4	2.5e−7	3	4e−6	0.25
	2.5e−7	3	4e−6	1
	2.5e−7	3	4e−6	1.75
	2.5e−7	3	4e−6	2.5
	2.5e−7	3	4e−6	3.25
5.3.5	2.5e−7	4	4e−6	0.25
	1.5e−6	1	4e−6	0.25
	2.75e−6	0.56	4e−6	0.25
	4e−6	038	4e−6	0.25
	5.25e−6	0.3	4e−6	0.25

5.3. Parametric study and performance evaluation

Specific cooling power (SCP) is defined as the ratio of evaporative cooling energy to the product of cycle time and dry sorbent mass. For the same sorbent mass, SCP represents the rapidity of the cool down/heat up processes mentioned in Section 5.2. To investigate various options to improve SCP, a parametric study on the oscillatory heat transfer characteristics including sorbent thermal diffusivity, HEX thermal diffusivity and thermal contact resistance, also on HEX to sorbent thickness ratio (HSTR) is con-

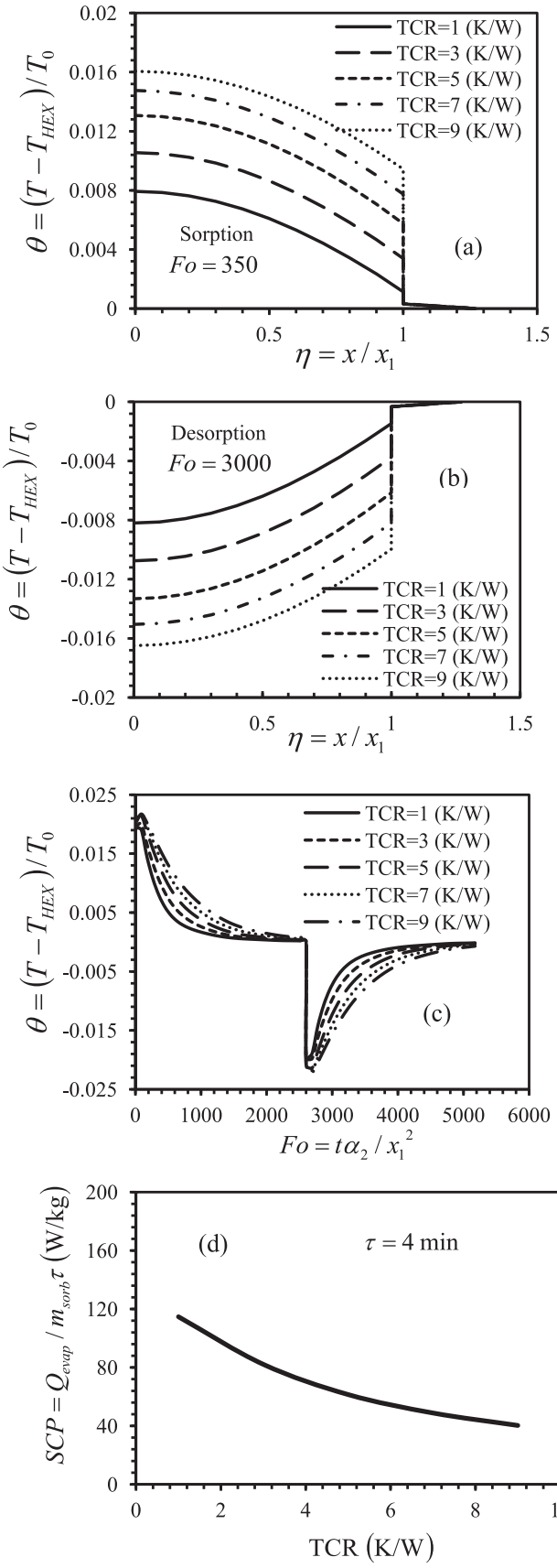

Fig. 8. Effect of thermal contact resistance on dimensionless temperature at (a) Fo = 350 (sorption phase), (b) Fo = 3000 (desorption phase), (c) η = 0, and (d) SCP.

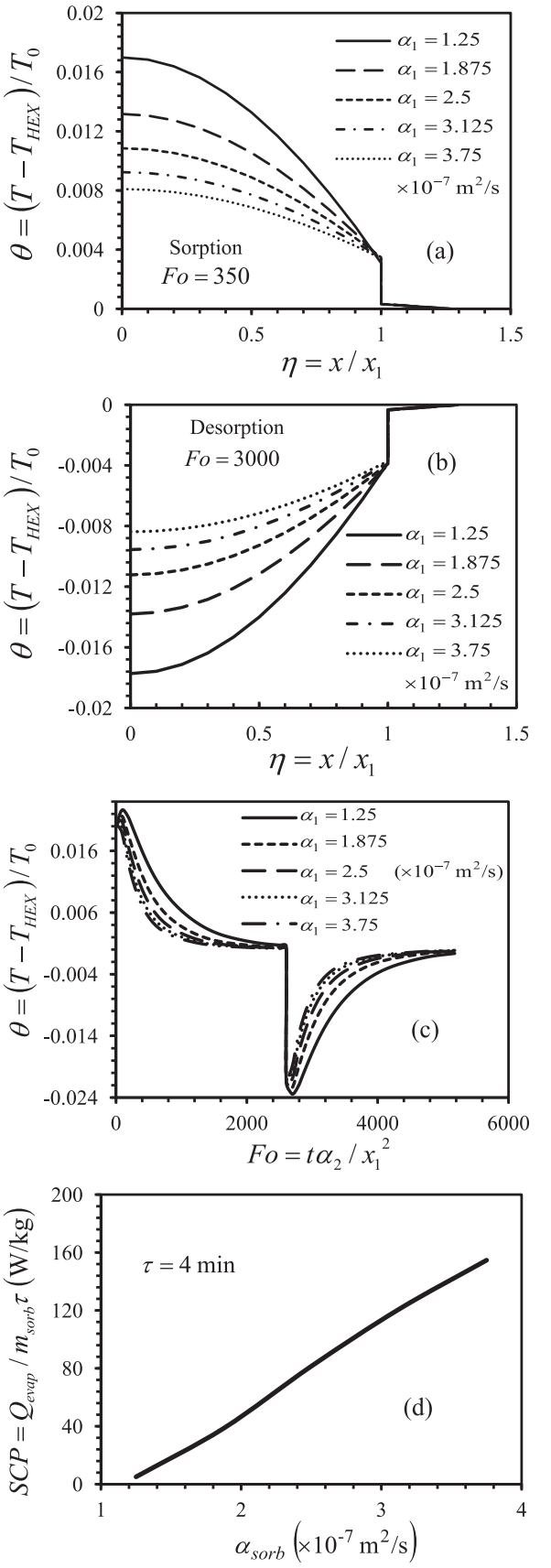

Fig. 9. Effect of sorbent thermal diffusivity on dimensionless temperature at (a) Fo = 350 (sorption phase), (b) Fo = 3000 (desorption phase), (c) η = 0, and (d) SCP.

ducted in this section. The different values of oscillatory heat transfer characteristics and geometrical specifications used for parametric study are presented in Table 2.

5.3.1. Effect of thermal contact resistance (TCR)

Fig. 8(a)–(c) shows the effect of thermal contact resistance on dimensionless temperature inside the sorber bed, see Table 2. It can be seen that the sorbent temperature decreases/increases during sorption/desorption by decreasing TCR as the temperature drop/jump at the sorbent-HEX interface decreases. Therefore, by reducing the TCR, the sorber bed can be cooled down/heated up faster during sorption/desorption phases; consequently, the SCP of the SCS will enhance (Fig. 8(d)).

5.3.2. Effect of sorbent thermal diffusivity

Fig. 9(a)–(c) shows the effect of sorbent thermal diffusivity on the dimensionless temperature inside the sorber bed, see Table 2. It shows that the sorbent temperature decreases/increases during sorption/desorption by increasing sorbent thermal diffusivity as the heat conduction in the sorbent enhances and the sorbent thermal inertia reduces. Hence, by increasing the sorbent thermal diffusivity, the cool down/heat up processes of sorber bed are accelerated during sorption/desorption phases, thereby enhancing the SCP of the SCS (Fig. 9(d)).

5.3.3. Effect of HEX thermal diffusivity

Fig. 10 shows the variation of SCP with HEX thermal diffusivity, see Table 2. It is evident that the thermal diffusivity of such thin HEX has insignificant impact on SCP as the heat transfer performance is limited by the low sorbent thermal diffusivity and high TCR at sorbent/HEX interface.

5.3.4. Effect of HEX to sorbent thickness ratio (HSTR)

Fig. 11(a)–(c) shows the effect of HSTR on the dimensionless temperature inside the sorber bed, see Table 2. It shows that the bed temperature decreases/increases during sorption/desorption by decreasing HSTR because the relative thermal resistance of HEX to sorbent as well as the relative thermal inertia of HEX to sorbent reduce. Hence, decrease of HSTR hastens the cool down/heat up processes of sorber bed during sorption/desorption phases, which means a higher SCP of SCS (Fig. 11(d)).

5.3.5. Effect of sorbent thermal diffusivity and TCR

Fig. 12 shows the effect of sorbent thermal diffusivity in conjunction with TCR on the SCP of the SCS studied in this paper, see Table 2. When the sorbent–HEX TCR remains constant and α_{sorb}

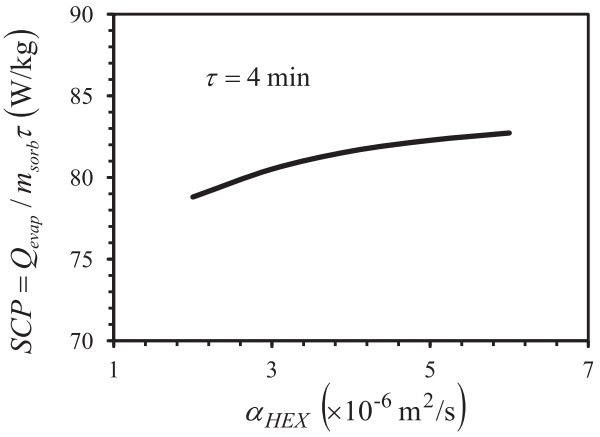

Fig. 10. Effect of HEX thermal diffusivity on SCP of SCS.

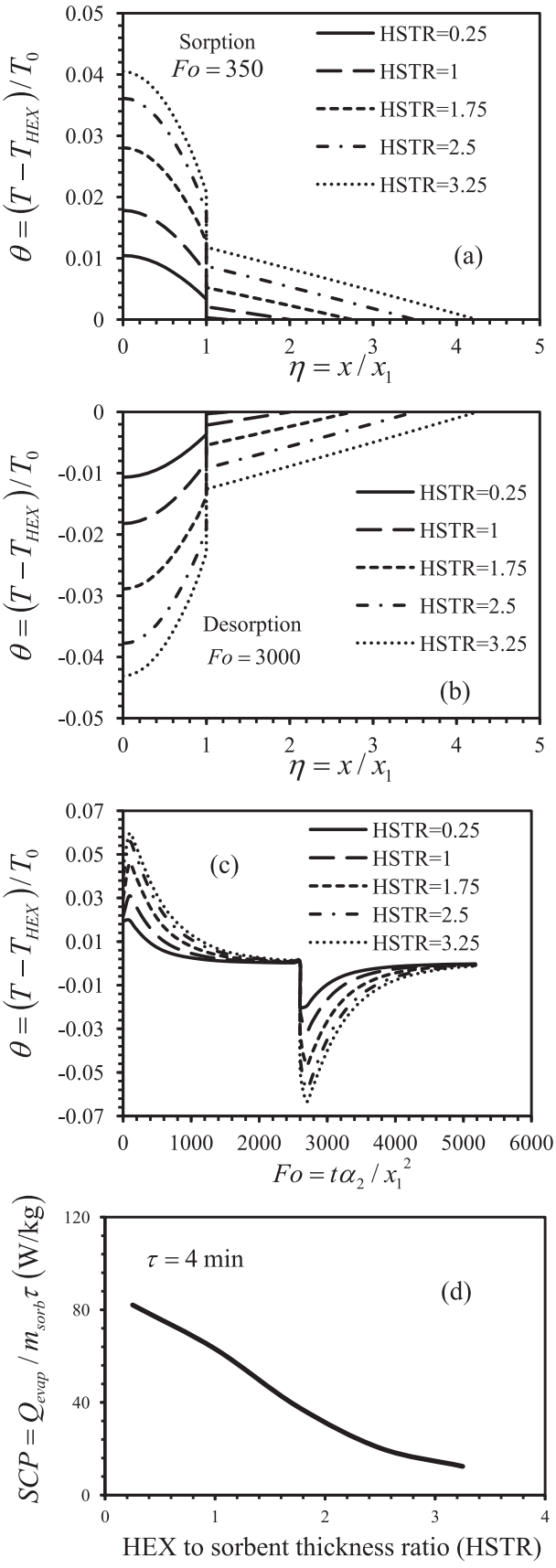

Fig. 11. Effect of HEX to sorbent thickness ratio (HSTR) on dimensionless temperature at (a) Fo = 350 (sorption phase), (b) Fo = 3000 (desorption phase), (c) η = 0, and (d) SCP.

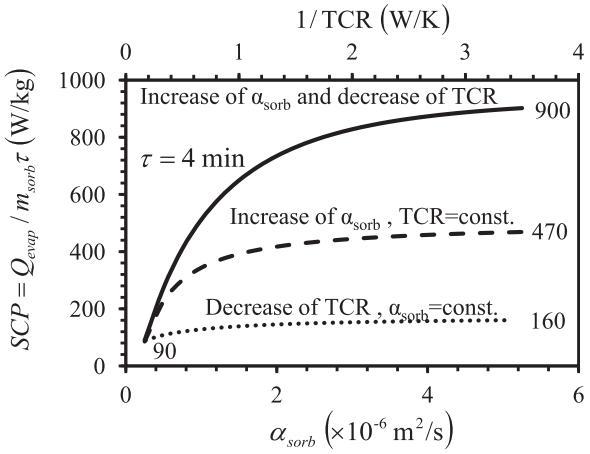

Fig. 12. Effect of sorbent thermal diffusivity and TCR on SCP.

increases, the improvement of SCP is much higher compared to the case where α_{sorb} remains constant and TCR reduces; hence, α_{sorb} has a higher impact on the SCP compared to TCR. However, simultaneous increase of α_{sorb} and decrease of TCR results in remarkable enhancement of the SCP. For example, SCP increases from 90 to 900 W/kg, (an order of magnitude) by increasing the sorbent thermal diffusivity from 2.5e to 7 to 5.25e−6 (m^2/s) and decreasing the TCR from 4 to 0.3 (K/W). Therefore, both sorbent thermal diffusivity and TCR should be improved to enhance the SCS performance.

6. Conclusions

A novel analytical model was developed to study the oscillatory heat transfer in sorber beds. A new gravimetric large pressure jump (GLAP) test bed was designed in which large sample uptake measurements were performed and validated against TGA uptake values. A number of new graphite coated sorption beds were prepared and tested in the GLAP test bed. The model was successfully validated with the experimental data obtained with the GLAP test bed. The temperature drop values of sorbent, sorbent-HEX TCR and the HEX are found to make up 69%, 28% and 3%, respectively, of the total temperature drop inside the sorber bed. It was found that the sorbent thermal diffusivity, TCR at the sorbent–HEX interface and HSTR had large impacts on the performance of an SCS. Thus, by enhancing the sorbent thermal diffusivity, reducing the TCR and using thin graphite sheets, the performance and SCP of SCS can be improved remarkably.

Conflict of interest

The authors declared that there is no conflict of interest.

Acknowledgement

The first author thanks the LAEC members, Khorshid Fayazmanesh, PhD candidate, Dr. Claire McCague, postdoctoral fellow, and Dr. Wendell Huttema, lab engineer, for building GLAP test bed and preparing sorbent materials required to run the experiments. Furthermore, the authors gratefully acknowledge the financial support of the Natural Sciences and Engineering Research Council of Canada (NSERC) through the Automotive Partnership Canada Grant No. APCPJ 401826-10.

Appendix A

Based on Eqs. (8)–(12), the following eigen-value problem can be established [32].

$$\mu_i \frac{d^2 X_{in}(\eta)}{d\eta^2} + \beta_n^2 X_{in}(\eta) = 0 \tag{A1}$$

$$\frac{dX_{1n}(0)}{d\eta} = 0 \tag{A2}$$

$$\frac{dX_{1n}(1)}{d\eta} = \kappa_2 \frac{dX_{2n}(1)}{d\eta} \tag{A3}$$

$$-\frac{dX_{1n}(1)}{d\eta} = \frac{1}{R_c}(X_{1n}(1) - X_{2n}(1)) \tag{A3}$$

$$X_{2n}(x_2/x_1) = 0 \tag{A4}$$

The following transcendental equation is obtained to evaluate the eigenvalues.

$$\begin{aligned}&\frac{1}{R_c\sqrt{\mu_1}}\tan\left(\frac{\beta_n}{\sqrt{\mu_2}}\right)\tan\left(\frac{\beta_n}{\sqrt{\mu_1}}\right) - \frac{\kappa_1\beta_n}{\sqrt{\mu_1}\sqrt{\mu_2}}\tan\left(\frac{\beta_n}{\sqrt{\mu_1}}\right) + \frac{\kappa_1}{R_c\sqrt{\mu_2}}\\ &- \frac{1}{R_c\sqrt{\mu_1}}\tan\left(\frac{\beta_n x_2}{\sqrt{\mu_2}x_1}\right)\tan\left(\frac{\beta_n}{\sqrt{\mu_1}}\right) - \frac{\kappa_1\beta_n}{\sqrt{\mu_1}\sqrt{\mu_2}}\tan\left(\frac{\beta_n x_2}{\sqrt{\mu_2}x_1}\right)\\ &\times\tan\left(\frac{\beta_n}{\sqrt{\mu_2}}\right)\tan\left(\frac{\beta_n}{\sqrt{\mu_1}}\right) + \frac{\kappa_1}{R_c\sqrt{\mu_2}}\tan\left(\frac{\beta_n x_2}{\sqrt{\mu_2}x_1}\right)\tan\left(\frac{\beta_n}{\sqrt{\mu_2}}\right) = 0\end{aligned} \tag{A5}$$

Eigenfunctions associated with each eigenvalue are given by Eqs. (A6) and (A7).

$$X_{1n}(\eta) = \cos\left(\frac{\beta_n}{\sqrt{\mu_1}}\eta\right) \tag{A6}$$

$$X_{2n}(\eta) = C_{2n}\cos\left(\frac{\beta_n}{\sqrt{\mu_2}}\eta\right) + D_{2n}\sin\left(\frac{\beta_n}{\sqrt{\mu_2}}\eta\right) \tag{A7}$$

$$D_{2n} = \frac{\sqrt{\mu_2}\sin\left(\frac{\beta_n}{\sqrt{\mu_1}}\right)}{-\kappa_1\sqrt{\mu_1}\left(\sin\left(\frac{\beta_n}{\sqrt{\mu_2}}\right)\tan\left(\frac{\beta_n x_2}{\sqrt{\mu_2}x_1}\right) + \cos\left(\frac{\beta_n}{\sqrt{\mu_2}}\right)\right)} \tag{A8}$$

$$C_{2n} = -D_{2n}\tan\left(\frac{\beta_n x_2}{\sqrt{\mu_2}x_1}\right) \tag{A9}$$

Assuming that initial condition satisfies Dirichlet's condition, this function can be expanded over the entire range of two layers in an infinite series of eigenfunctions in the form:

$$f_i(\eta) = \sum_{n=1}^{\infty} f_n^* X_{in}(\eta) \tag{A10}$$

Unity can also be expanded:

$$I = \sum_{n=1}^{\infty} I_n^* X_{in}(\eta) \tag{A11}$$

Using the orthogonal property of eigenfunctions (Eq. (A12)), Eqs. (A13)(A15) can be acquired.

$$\sum_{i=1}^{m}\frac{\kappa_i}{\mu_i}\int_{x_i}^{x} X_{in}(\eta)X_{in'}(\eta)d\eta = \begin{cases} 0 & for\ n \neq n' \\ const. & for\ n = n' \end{cases} \tag{A12}$$

$$\begin{aligned}f_n^* &= \frac{1}{N}\sum_{i=1}^{m}\frac{\kappa_i}{\mu_i}\int_{x_i}^{x_{i+1}} f_i(\eta)X_{in}(\eta)d\eta\\ &= \frac{\kappa_1(T_{1,0} - T_{HEX}(0))}{N\sqrt{\mu_1}\beta_n T_{2,0}}\sin\left(\frac{\beta_n}{\sqrt{\mu_1}}\right)\\ &+ \frac{\kappa_2(T_{2,0} - T_{HEX}(0))}{N\sqrt{\mu_2}\beta_n T_{2,0}}\left(C_{2n}\sin\left(\frac{\beta_n}{\sqrt{\mu_2}}\frac{x_2}{x_1}\right) - D_{2n}\left(\cos\left(\frac{\beta_n}{\sqrt{\mu_2}}\frac{x_2}{x_1}\right) - 1\right)\right)\end{aligned} \tag{A13}$$

$$I_n^* = \frac{1}{N}\sum_{i=1}^{m}\frac{\kappa_i}{\mu_i}\int_{x_i}^{x_{i+1}} X_{in}(\eta)d\eta = \frac{1}{N}\frac{\sqrt{\mu_1}}{\beta_n}\sin\left(\frac{\beta_n}{\sqrt{\mu_1}}\right) + \frac{1}{N}\frac{\kappa_2 C_{2n}}{\sqrt{\mu_2}\beta_n}\left(\sin\left(\frac{\beta_n x_2}{\sqrt{\mu_2}x_1}\right) - \sin\left(\frac{\beta_n}{\sqrt{\mu_2}}\right)\right) - \frac{1}{N}\frac{\kappa_2 D_{2n}}{\sqrt{\mu_2}\beta_n}\left(\cos\left(\frac{\beta_n x_2}{\sqrt{\mu_2}x_1}\right) - \cos\left(\frac{\beta_n}{\sqrt{\mu_2}}\right)\right) \tag{A14}$$

$$N = \sum_{i=1}^{m}\frac{\kappa_i}{\mu_i}\int_{x_i}^{x_{i+1}} X_{in}^2(\eta)d\eta = \frac{1}{2}\left(1 + \frac{\sqrt{\mu_1}}{2\beta_n}\sin\left(\frac{2\beta_n}{\sqrt{\mu_1}}\right)\right) + \frac{\kappa_2}{\mu_2}\begin{pmatrix} \frac{1}{2}C_{2n}^2\left(\frac{x_2}{x_1} - 1 + \frac{\sqrt{\mu_2}}{2\beta_n}\left(\sin\left(\frac{2\beta_n x_2}{\sqrt{\mu_2}x_1}\right) - \sin\left(\frac{2\beta_n}{\sqrt{\mu_2}}\right)\right)\right) \\ + \frac{1}{2}D_{2n}^2\left(\frac{x_2}{x_1} - 1 - \frac{\sqrt{\mu_2}}{2\beta_n}\left(\sin\left(\frac{2\beta_n x_2}{\sqrt{\mu_2}x_1}\right) - \sin\left(\frac{2\beta_n}{\sqrt{\mu_2}}\right)\right)\right) \\ - \frac{\sqrt{\mu_2}}{2\beta_n}C_{2n}D_{2n}\left(\cos\left(\frac{2\beta_n x_2}{\sqrt{\mu_2}x_1}\right) - \cos\left(\frac{2\beta_n}{\sqrt{\mu_2}}\right)\right) \end{pmatrix} \tag{A15}$$

Substituting Eq. (A16) into Eq. (8) and some algebraic manipulation, Eq. (A17) can be derived.

$$\theta_i(\eta, Fo) = \sum_{n=1}^{\infty} X_{in}(\eta)\Gamma_n(Fo) \tag{A16}$$

$$\frac{d\Gamma_n(Fo)}{dFo} + \beta_n^2\Gamma_n(Fo) = -\frac{1}{T_0}I_n^*\frac{dT_{HEX}(Fo)}{dFo} \tag{A17}$$

$$f_i(\eta) = \sum_{n=1}^{\infty} X_{in}(\eta)\Gamma_n(0) \tag{A18}$$

$$\Gamma_n(0) = f_n^* \tag{A19}$$

The answer to the above ordinary differential equation is

$$\Gamma_n(Fo) = e^{-\beta_n^2 Fo}\left(f_n^* + \int_{Fo'=0}^{Fo'=Fo}\left[-\frac{1}{T_0}I_n^*\frac{dT_{HEX}(Fo')}{dFo'}\right]e^{\beta_n^2 Fo'}dFo'\right) \tag{A20}$$

References

[1] Building Energy Data Book, 2012. U.S. Dep. Energy.
[2] W. Wu, H. Zhang, D. Sun, Mathematical simulation and experimental study of a modified zeolite 13X–water adsorption refrigeration module, Appl. Therm. Eng. 29 (2009) 645–651.
[3] Y. Zhao, E. Hu, A. Blazewicz, Dynamic modelling of an activated carbon–methanol adsorption refrigeration tube with considerations of interfacial convection and transient pressure process, Appl. Energy 95 (2012) 276–284.
[4] A. Sharafian, C. McCague, M. Bahrami, Impact of fin spacing on temperature distribution in adsorption cooling system for vehicle A/C applications, Int. J. Refrig. 51 (2015) 135–143.
[5] A. Freni, B. Dawoud, L. Bonaccorsi, S. Chmielewski, A. Frazzica, L. Calabrese, G. Restuccia, Characterization of Zeolite-Based Coatings for Adsorption Heat Pumps, Springer International Publishing, Cham, 2015.
[6] A. Sharafian, K. Fayazmanesh, C. Mccague, M. Bahrami, Thermal conductivity and contact resistance of mesoporous silica gel adsorbents bound with polyvinylpyrrolidone in contact with a metallic substrate for adsorption cooling system applications, Int. J. Heat Mass Transf. 79 (2014) 64–71.
[7] A. Rezk, R.K. Al-Dadah, S. Mahmoud, A. Elsayed, Effects of contact resistance and metal additives in finned-tube adsorbent beds on the performance of silica gel/water adsorption chiller, Appl. Therm. Eng. 53 (2) (2013) 278–284.
[8] L. Yong, K. Sumathy, Review of mathematical investigation on the closed adsorption heat pump and cooling systems, Renew. Sustain. Energy Rev. 6 (2002) 305–337.
[9] G. Cacciola, G. Restuccia, Reversible adsorption heat pump: a thermodynamic model, Int. J. Refrig. 18 (2) (1995) 100–106.
[10] S. Henninger, M. Schicktanz, P. Hugenell, H. Sievers, H. Henning, Evaluation of methanol adsorption on activated carbons for thermally driven chillers, Part I: Thermophysical characterisation, Int. J. Refrig. 35 (2012) 543–553.
[11] E. Anyanwu, N. Ogueke, Thermodynamic design procedure for solid adsorption solar refrigerator, Renew. Energy 30 (2005) 81–96.
[12] Z. Tamainot-Telto, S.J. Metcalf, R.E. Critoph, Y. Zhong, R. Thorpe, Carbon – ammonia pairs for adsorption refrigeration applications: ice making, air conditioning and heat pumping, Int. J. Refrig. 32 (6) (2009) 1212–1229.
[13] S. Vasta, G. Maggio, G. Santori, A. Freni, F. Polonara, G. Restuccia, An adsorptive solar ice-maker dynamic simulation for north Mediterranean climate, Energy Convers. Manage. 49 (2008) 3025–3035.
[14] N. Khattab, Simulation and optimization of a novel solar-powered adsorption refrigeration module, Sol. Energy 80 (2006) 823–833.
[15] M. Umair, A. Akisawa, Y. Ueda, Performance evaluation of a solar adsorption refrigeration system with a wing type compound parabolic concentrator, Energies 7 (2014) 1448–1466.
[16] B. Saha, I. El-Sharkawy, A. Chakraborty, S. Koyama, Study on an activated carbon fiber-ethanol adsorption chiller: Part I – System description and modelling, Int. J. Refrig. 30 (2007) 86–95.
[17] B. Saha, I. El-Sharkawy, A. Chakraborty, S. Koyama, Study on an activated carbon fiber-ethanol adsorption chiller: Part II – Performance evaluation, Int. J. Refrig. 30 (2007) 96–102.
[18] R. Ahmed, R. Al-Dadah, Physical and operating conditions effects on silica gel/water adsorption chiller performance, Appl. Energy 89 (2012) 142–149.
[19] K.C.A. Alam, B.B. Saha, Y.T. Kang, A. Akisawa, T. Kashiwagi, Heat exchanger design effect on the system performance of silica gel adsorption refrigeration systems, Int. J. Heat Mass Transf. 43 (2000) 4419–4431.
[20] L. Marletta, G. Maggio, A. Freni, M. Ingrasciotta, G. Restuccia, A non-uniform temperature non-uniform pressure dynamic model of heat and mass transfer in compact adsorbent beds, Int. J. Heat Mass Transf. 45 (16) (2002) 3321–3330.
[21] G.G. Ilis, M. Mobedi, S. Ülkü, A dimensionless analysis of heat and mass transport in an adsorber with thin fins; uniform pressure approach, Int. Commun. Heat Mass Transf. 38 (2011) 790–797.
[22] I. Solmuş, D.A.S. Rees, C. Yamal, D. Baker, B. Kaftanoğlu, Numerical investigation of coupled heat and mass transfer inside the adsorbent bed of an adsorption cooling unit, Int. J. Refrig. 35 (2012) 652–662.
[23] I. Solmus, D. Andrew, S. Rees, C. Yamalı, D. Baker, A two-energy equation model for dynamic heat and mass transfer in an adsorbent bed using silica gel/water pair, Int. J. Heat Mass Transf. 55 (2012) 5275–5288.
[24] A.O. Yurtsever, G. Karakas, Y. Uludag, Modeling and computational simulation of adsorption based chemical heat pumps, Appl. Therm. Eng. 50 (2013) 401–407.
[25] A. Mhimid, Theoretical study of heat and mass transfer in a zeolite bed during water desorption: validity of local thermal equilibrium assumption, Int. J. Heat Mass Transf. 41 (19) (1998) 2967–2977.
[26] K.C. Leong, Y. Liu, Numerical study of a combined heat and mass recovery adsorption cooling cycle, Int. J. Heat Mass Transf. 47 (22) (2004) 4761–4770.
[27] H. Niazmand, I. Dabzadeh, Numerical simulation of heat and mass transfer in adsorbent beds with annular fins, Int. J. Refrig. 35 (2012) 581–593.
[28] Y.L. Zhao, E. Hu, A. Blazewicz, A non-uniform pressure and transient boundary condition based dynamic modeling of the adsorption process of an adsorption refrigeration tube, Appl. Energy 90 (1) (2012) 280–287.
[29] M. Mahdavikhah, H. Niazmand, Effects of plate finned heat exchanger parameters on the adsorption chiller performance, Appl. Therm. Eng. 50 (2013) 939–949.
[30] Q.W. Pan, R.Z. Wang, L.W. Wang, Comparison of different kinds of heat recoveries applied in adsorption refrigeration system, Int. J. Refrig. 55 (2015) 37–48.
[31] E. Anyanwu, N.V. Ogueke, Transient analysis and performance prediction of a solid adsorption solar refrigerator, Appl. Therm. Eng. 27 (2007) 2514–2523.
[32] M.N. Ozisik, Boundary Value Problem of Heat Conduction, International Textbook, London, 1968.